ChemComm

Quantifying effects of second-sphere cationic groups on redox properties of dimolybdenum quadruple bonds

Journal:	*ChemComm*
Manuscript ID	CC-COM-06-2024-002759.R1
Article Type:	Communication

COMMUNICATION

Quantifying effects of second-sphere cationic groups on redox properties of dimolybdenum quadruple bonds†

Received 00th January 20xx,
Accepted 00th January 20xx

DOI: 10.1039/x0xx00000x

S. M. Supundrika Subasinghe[a] and Neal P. Mankad*[a]

A series of four dimolybdenum paddlewheel complexes supported by anionic *N*,*N*-dimethylglycinate (DMG) or zwitterionic *N*,*N*,*N*-trimethylglycine (TMG) ligands was synthesised to examine the effects of charged groups in the second coordination sphere on redox properties of Mo≣Mo bonds. An average shift in reduction potential of +35 mV per cationically charged group was measured, which is approximately half of what would be expected for an analogous mononuclear complex.

Electrostatic fields controlling the properties of an active site is seen in nature[1] and used in both molecular and heterogeneous catalyst systems.[2–12] Therefore, studies that quantify electrostatic field effects on metal active sites are valuable. Several studies have done so on mononuclear metal sites through the use of charged groups[13–16] or alkali metal binding sites[17–21] in the second coordination sphere. For example, Wang has studied ferrocene derivatives bearing either cationic or anionic groups in the second coordination sphere (Figure 1a).[15,16] The resulting changes to Fe^{III}/Fe^{II} reduction potential and to molecular solubility were found to be useful in the context of non-aqueous redox flow batteries.

Comparatively fewer studies have quantified the effects of electrostatic fields on binuclear or multinuclear metal complexes,[22–24] even though such measurements would be relevant to bioinorganic[1] and heterogeneous[7–9] systems that often employ clusters or extended arrays of metal atoms. We hypothesized that quadruply-bonded paddlewheel complexes,[25,26] a canonical example of which is $Mo_2(OAc)_4$, would be a suitable platform to conduct such measurements. Some advantages of the platform include: (a) convenient substitution of the bridging paddlewheel ligands via extensively mapped synthetic protocols;[27,28] (b) well-behaved and reversible redox chemistry associated with the δ electrons;[29] and (c) established primary coordination sphere effects on redox behaviour[30,31] that enable focus on secondary coordination sphere effects here. Thus, herein we provide quantification of the effects of second-sphere cationic groups on the $[Mo_2]^{5+}/[Mo_2]^{4+}$ reduction potentials of paddlewheel complexes that featuring bridging *N*,*N*-dimethylglycinate (DMG) anions and their zwitterionic counterpart, *N*,*N*,*N*-trimethylglycine (TMG) (Figure 1b). The pK_a values of DMG and TMG are 2.04 and 1.83, respectively,[32,33] indicating that they should have similar donor strengths in the primary coordination sphere and enable isolation of secondary coordination sphere effects in a systematic study. Along these lines, the partial atomic charges of the oxygen atoms were calculated to be nearly identical computationally (see ESI).

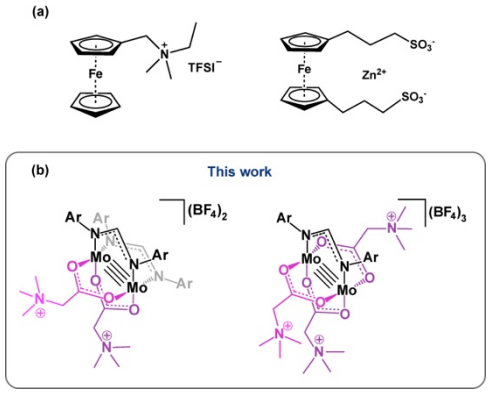

Figure 1. Second-sphere charged groups affecting reduction potentials in: (a) previously studied, mononuclear ferrocene derivatives (TFSI = $N[SO_2CF_3]_2$); and (b) Mo≣Mo complexes reported here.

[a] *Department of Chemistry, University of Illinois Chicago, Chicago, IL 60607 (USA)*
† Electronic Supplementary Information (ESI) available: experimental section, spectral characterization data, additional cyclic voltammetry plots, computational output. See DOI: 10.1039/x0xx00000x
*E-mail: npm@uic.edu

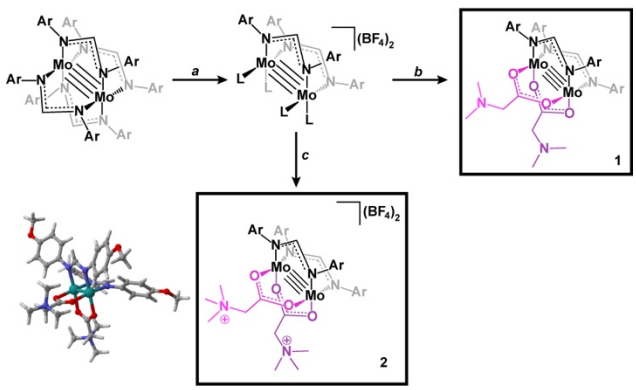

Scheme 1. Synthesis of *cis*-$Mo_2(DAniF)_2(DMG)_2$ (**1**) and *cis*-$[Mo_2(DAniF)_2(TMG)_2][BF_4]_2$ (**2**). Reaction conditions (all at room temperature): (a) $[Et_3O][BF_4]$(4.0 equiv.), H_2O (trace), CH_3CN, overnight; (b) Li[DMG] (3.5 equiv.), CH_3CN, 2 h; (c) TMG (3.5 equiv.), CH_3CN, 2 h. L = CH_3CN and Ar = *p*-$C_6H_4OCH_3$. The calculated of **2** is shown alongside its drawing.

An initial pair of complexes for investigation was prepared as shown in Scheme 1. Following established literature protocols,[28] $Mo_2(DAniF)_4$ was converted to the synthon, *cis*-$[Mo_2(DAniF)_2(CH_3CN)_4][BF_4]_2$ (DAniF = *N*,*N*'-di-*p*-anisylformamidinate). Subsequent addition of Li[DMG] or TMG produced yellow-coloured *cis*-$Mo_2(DAniF)_2(DMG)_2$ (**1**) and *cis*-$[Mo_2(DAniF)_2(TMG)_2][BF_4]_2$ (**2**) in 87% and 84% yields, respectively. Both complexes are highly soluble in CH_3CN, acetone, and MeOH but insoluble in THF. Although we were unable to obtain crystals suitable for X-ray diffraction, we obtained optimized structures from DFT calculations. The calculated average distance from the quaternary nitrogen centres to the Mo_2 midpoint of 5.12 Å. The calculated Mo≡Mo distances for **1** and **2** are 2.074 and 2.071 Å, respectively.

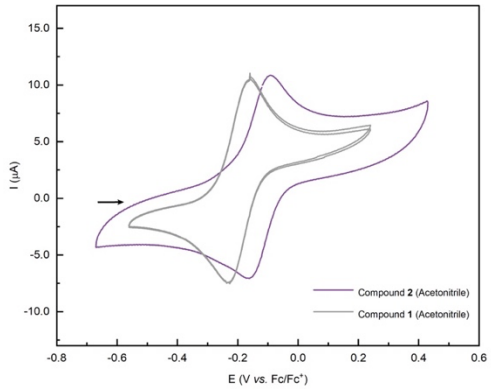

Figure 2. Cyclic voltammograms for **1** and **2** (1.5 mM) at 100 mV s^{-1} in 0.1 M $[Bu_4N][PF_6]$ in CH_3CN.

The cyclic voltammograms (CVs) of **1** and **2** were collected using $[Bu_4N][PF_6]$ as the supporting electrolyte in both acetone and acetonitrile to probe the influence of solvent dielectric on any electrostatic effect. Data obtained in acetonitrile is presented here, and acetone data is given in ESI. Both complexes featured reversible redox events assigned to $[Mo_2]^{5+}/[Mo_2]^{4+}$ processes (Figure 2). Complex **1** showed a half-wave potential ($E_{1/2}$) of -0.198 V, while **2** was shifted to -0.128 V (Table 1, all potentials reported vs. $FeCp_2^{+/0}$). This 70-mV shift is attributed to the introduction of two positively charged groups in **2**. As expected for a less polar solvent that reduces shielding of the electrostatic field, the shift was increased to 115 mV in acetone. However, whereas **2** was anodically shifted from **1** in acetonitrile, the shift was cathodic in acetone. Based on this observation, it seems that the solvent dielectric has a mild impact on the potential of neutral **1** but a strong impact on the potential of dicationic **2**. We also repeated the experiments with $[Bu_4N][OTf]$ and $[Bu_4N][B(C_6F_5)_4]$ as supporting electrolytes in place of $[Bu_4N][PF_6]$. As expected,[34] the shift in potential between neutral **1** and cationic **2** was found to be anion-dependent, but the differences were subtle, ranging from 20 mV for ^-OTf to 70 mV for PF_6^- (see Figure S14).

Table 1. Electrochemical values for **1**-**4**.[a]

Entry	Compound	E_{pc} (V)	E_{pa} (V)	$E_{1/2}$ (V)[b]
1	*cis*-$Mo_2(DAniF)_2(DMG)_2$	-0.163	-0.233	-0.198
2	*cis*-$Mo_2(DAniF)_2(TMG)_2^{2+}$	-0.163	-0.094	-0.128
3	$Mo_2(DAniF)(DMG)_3$	0.144	0.059	0.102
4	$Mo_2(DAniF)(TMG)_3^{3+}$	0.238	0.154	0.196

[a] All potentials are referenced to ferrocene as recorded in acetonitrile solvent with $[Bu_4N][PF_6]$ supporting electrolyte. [b] $E_{1/2} = (E_{pc} + E_{pa})/2$.

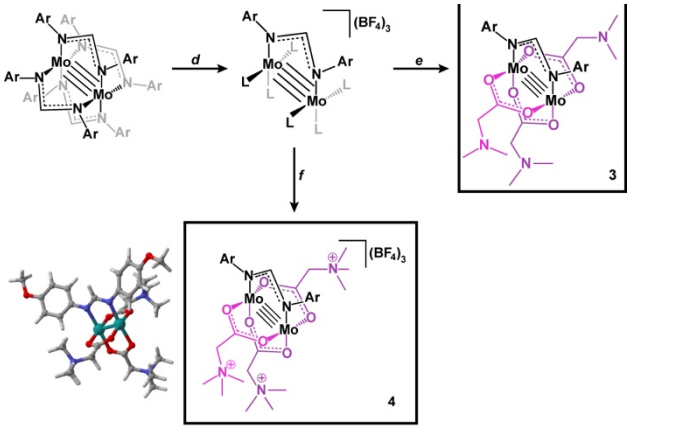

Scheme 2. Synthesis of $Mo_2(DAniF)(DMG)_3$ (**3**) and $[Mo_2(DAniF)(TMG)_3][BF_4]_3$ **(4).** Reaction conditions (all at room temperature): (d) $HBF_4{\cdot}OEt_2$ (5.5 equiv.), CH_2Cl_2:CH_3CN (4:1), 0.5 h; (e) Li[DMG] (5 equiv.), CH_3CN, 12 h; (f) TMG (5 equiv.), CH_3CN, 12 h. L = CH_3CN and Ar = p-$C_6H_4OCH_3$. The calculated structure of **4** is shown alongside its drawing.

Next, we targeted tris(substituted) derivatives (Scheme 2). According to literature procedures,[28] $Mo_2(DAniF)_4$ was converted to the synthon, $[Mo_2(DAniF)(CH_3CN)_6][BF_4]_3$. Subsequent addition of Li[DMG] or TMG produced yellow compounds $Mo_2(DAniF)(DMG)_3$ (**3**) and $[Mo_2(DAniF)(TMG)_3][BF_4]_3$ (**4**) in 83% and 89% yields, respectively. Both **3** and **4** show similar solubility and thermal stability properties as **1** and **2**. Interestingly, the room-temperature ^1H NMR spectra for **3** and **4** each exhibit a single set of resonances for DMG and TMG, respectively. At lower temperatures (Figures 3 and S10), the chemical shifts and linewidths of these resonances showed variations, and de-coalescence was observed for **4** at 245 K. We interpret these observations as being indicative of dynamic interconversion of the *cis*- and *trans*-ligands in **3** and **4**. This type of fluxionality was

not previously observed for $Mo_2(DAniF)(OAc)_3$.[35] Once again, we were unable to obtain crystal structures of these complexes but analysed their optimized structures from DFT calculations. The calculated average $Mo_2\cdots NR_4^+$ distance of 5.14 Å, which is very similar to the value for **2**. The calculated Mo≡Mo distances for **3** and **4** are 2.062 and 2.067 Å, respectively.

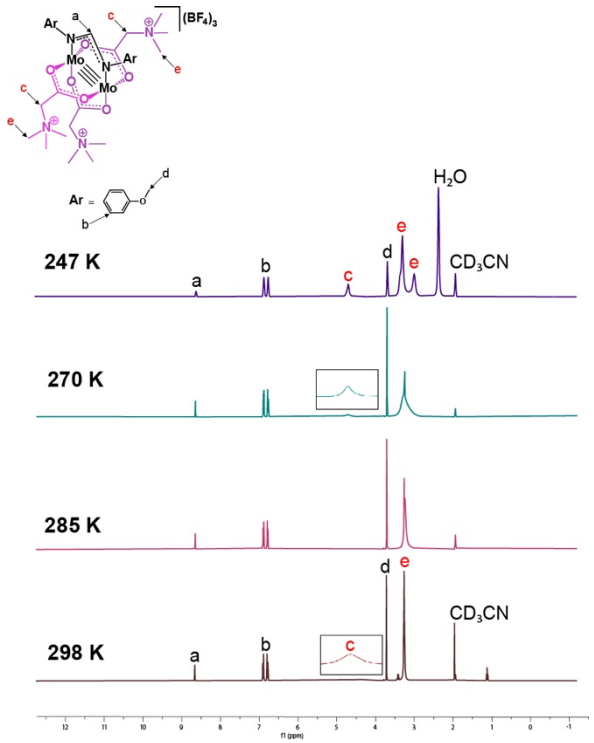

Figure 3. ^{1}H NMR spectra for compound **4** at different temperatures.

Analysis of **3** and **4** by CV (Figure S15) in acetonitrile revealed a difference in redox potentials of 95 mV, which can be attributed to the introduction of three positively charged groups in **4**. Curiously, in this case, a smaller shift of 30 mV was observed in acetone. Comparing the CVs of the two cationic complexes, **2** and **4**, showed a more pronounced shift of 324 mV in acetonitrile (Figure 4), which increased slightly to 400 mV in acetone. On the other hand, examining the two uncharged complexes, **1** and **3**, showed that **3** is shifted to more positive potentials by 300 mV in acetonitrile (285 mV in acetone, Figures S16-20). Thus, of the 324-mV positive shift from **2** to **4**, 300 mV can be attributed to the primary-sphere effect of replacing DAniF with a glycinate and 24 mV is due to the second-sphere effects of the one additional cationic group in **4**. We were unable to probe the effect of electrolyte composition for this pair, since the addition of $[Bu_4N][OTf]$ or $[Bu_4N][B(C_6F_5)_4]$ to **4** caused decomposition and precipitation of the compound.

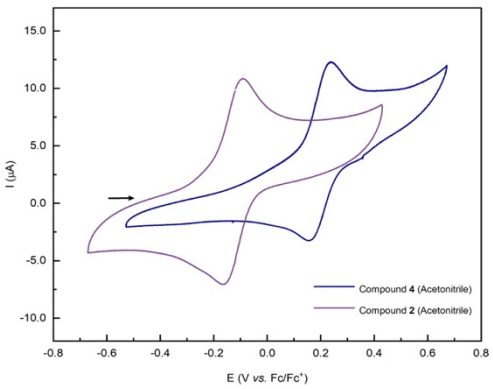

Figure 4. Cyclic voltammograms for **2** and **4** (1.5 mM) at 100 mV s^{-1} in 0.1 M $[Bu_4N][PF_6]$ in CH_3CN.

Collecting these observations together, there is an observed linear correlation between the number of added cationic groups and the shift in $E_{1/2}$ derived from data obtained in acetonitrile (Figure 5a). The slope of the line is +35 ± 5 mV per cation. This is significantly smaller than the +230 mV per cation and -180 to -230 mV per anion observed by Wang for ferrocene derivatives (Figure 1a),[15,16] which were in line with other studies with mononuclear metal complexes bearing charged groups. Thus, we can conclude that the binuclear, quadruply-bonded $[Mo_2]^{n+}$ unit is relatively insensitive to the electrostatic field induced by second-sphere charges, which may be partly due to the somewhat long $Mo_2\cdots NR_4^+$ distances. Unlike the acetonitrile data set, no correlation was obtained from the acetone data.

For mononuclear metal complexes featuring pendant charges, the change in electrostatic field potential has been analysed according to equation 1,[21] where q is the Coulombic charge of the pendant group Q^{n+}, ε is the dielectric constant (multiplied by vacuum permittivity, see ESI), and r is the $M\cdots Q^{n+}$ distance. This equation assumes that Q^{n+} is a point charge and that M is spherical. We became curious how well this model would apply to our system, where the approximately spherical M is replaced with a cylindrical M≡M unit. Thus, assuming a constant $Mo_2\cdots NR_4^+$ distance of 5.1 Å indicated by DFT calculations (see above), we calculated theoretical shifts in potential for the cases with 1, 2, and 3 pendant charges. Interestingly, plotting calculated vs. experimental shift in $E_{1/2}$ reveals a slope of 2.1 ± 0.3 (Figure 5b). In other words, even given the relatively long $Mo_2\cdots NR_4^+$ distances, the binuclear Mo_2 unit experiences an electrostatic field that is approximately half the magnitude of that experienced by analogous mononuclear metal centres. To our knowledge, this inverse correlation between electrostatic field and the number of metal centres has not been documented systematically in the literature. At this time, we cannot rule out other factors impacting the dependence of ΔE on q. For example, the $Mo_2\cdots NR_4^+$ distances may be dynamic in solution or underestimated by DFT, and counterion shielding may also play a role.

$$\Delta E = \frac{q}{4\pi\varepsilon r} \qquad \text{(eq 1)}$$

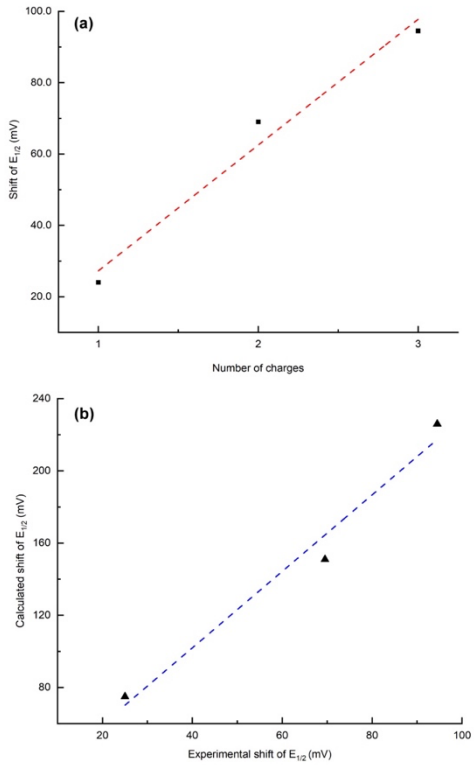

Figure 5. (a) Experimentally determined relationship between redox potential and second-sphere cationic charges (slope = 35 ± 5, intercept = -8 ± 12 with 95% confidence interval; R^2 = 0.982), (b) calculated vs. experimental shift in potential (slope = 2.11 ± 0.33, intercept = 0.017 ± 0.02 with 95% confidence interval; R^2 = 0.976).

This work was supported by the NSF through grant CHE-2350403. Dr. Dan McElheny (UIC) assisted with NMR spectroscopy. Computational resources were provided by the ACER group at UIC.

Data availability statement

Experimental section, supporting data, and computational output coordinates have been uploaded as ESI.

Conflicts of interest

There are no conflicts to declare.

Notes and references

1 A. Warshel, P. K. Sharma, M. Kato, Y. Xiang, H. Liu and M. H. M. Olsson, *Chem. Rev.*, 2006, **106**, 3210–3235.
2 D. H. Hall, L. E. Grove, C. Yueh, C. H. Ngan, D. Kozakov and S. Vajda, *J. Am. Chem. Soc.*, 2011, **133**, 20668–20671.
3 V. M. Lau, W. C. Pfalzgraff, T. E. Markland and M. W. Kanan, *J. Am. Chem. Soc.*, 2017, **139**, 4035–4041.
4 V. E. Anderson, *Arch. Biochem. Biophys.*, 2005, **433**, 27–33.
5 P. Hanoian, C. T. Liu, S. Hammes-Schiffer and S. Benkovic, *Acc. Chem. Res.*, 2015, **48**, 482–489.
6 C. Zheng, Z. Ji, I. I. Mathews and S. G. Boxer, *Nat. Chem.*, 2023, **15**, 1715–1721.
7 S. Ciampi, N. Darwish, H. M. Aitken, I. Díez-Pérez and M. L. Coote, *Chem. Soc. Rev.*, 2018, **47**, 5146–5164.
8 S.-J. Shin, H. Choi, S. Ringe, D. H. Won, H.-S. Oh, D. H. Kim, T. Lee, D.-H. Nam, H. Kim and C. H. Choi, *Nat. Commun.*, 2022, **13**, 5482.
9 S. Shaik, R. Ramanan, D. Danovich and D. Mandal, *Chem. Soc. Rev.*, 2018, **47**, 5125–5145.
10 S. D. Fried, S. Bagchi and S. G. Boxer, *Science*, 2014, **346**, 1510–1514.
11 M. E. Eberhart, T. R. Wilson, N. W. Johnston and A. N. Alexandrova, *J. Chem. Theory Comput.*, 2023, **19**, 694–704.
12 V. E. Anderson, M. W. Ruszczycky and M. E. Harris, *Chem. Rev.*, 2006, **106**, 3236–3251.
13 I. Azcarate, C. Costentin, M. Robert and J.-M. Savéant, *J. Am. Chem. Soc.*, 2016, **138**, 16639–16644.
14 W. Nie, D. E. Tarnopol and C. C. L. McCrory, *J. Am. Chem. Soc.*, 2021, **143**, 3764–3778.
15 X. Wei, L. Cosimbescu, W. Xu, J. Z. Hu, M. Vijayakumar, J. Feng, M. Y. Hu, X. Deng, J. Xiao, J. Liu, V. Sprenkle and W. Wang, *Adv. Energy Mater.*, 2015, **5**, 1400678.
16 L. Cosimbescu, X. Wei, M. Vijayakumar, W. Xu, M. L. Helm, S. D. Burton, C. M. Sorensen, J. Liu, V. Sprenkle and W. Wang, *Sci. Rep.*, 2015, **5**, 14117.
17 A. Santra, G. Gupta, B. Biswas, A. Das, D. Ghosh and S. Paria, *Inorg. Chem.*, 2023, **62**, 9818–9826.
18 T. Chantarojsiri, J. W. Ziller and J. Y. Yang, *Chem. Sci.*, 2018, **9**, 2567–2574.
19 T. Chantarojsiri, A. H. Reath and J. Y. Yang, *Angew. Chem. Int. Ed.*, 2018, **57**, 14037–14042.
20 K. Kang, J. Fuller, A. H. Reath, J. W. Ziller, A. N. Alexandrova and J. Y. Yang, *Chem. Sci.*, 2019, **10**, 10135–10142.
21 A. H. Reath, J. W. Ziller, C. Tsay, A. J. Ryan and J. Y. Yang, *Inorg. Chem.*, 2017, **56**, 3713–3718.
22 L. Grunwald, M. Clémancey, D. Klose, L. Dubois, S. Gambarelli, G. Jeschke, M. Wörle, G. Blondin and V. Mougel, *Proc. Natl. Acad. Sci.*, 2022, **119**, e2122677119.
23 S. Pattanayak, N. D. Loewen and L. A. Berben, *Inorg. Chem.*, 2022, **62**, 1919–1925.
24 P. Alayoglu, T. Chang, M. V. Lorenzo Ocampo, L. J. Murray, Y.-S. Chen and N. P. Mankad, *Inorg. Chem.*, 2023, **62**, 15267–15276.
25 F. A. Cotton, *Chem. Soc. Rev.*, 1975, **4**, 27–53.
26 S. Rej, H. Tsurugi and K. Mashima, *Coord. Chem. Rev.*, 2018, **355**, 223–239.
27 F. A. Cotton, C. Y. Liu and C. A. Murillo, *Inorg. Chem.*, 2004, **43**, 2267–2276.
28 M. H. Chisholm, F. A. Cotton, L. M. Daniels, K. Folting, J. C. Huffman, S. S. Iyer, C. Lin, A. M. Macintosh and C. A. Murillo, *J. Chem. Soc. - Dalton Trans.*, 1999, 1387–1391.
29 L. R. Falvello, B. M. Foxman and C. A. Murillo, *Inorg. Chem.*, 2014, **53**, 9441–9456.
30 N. Rodríguez-López, N. Metta, A. J. Metta-Magana and D. Villagrán, *Inorg. Chem.*, 2020, **59**, 3091–3101.
31 C. Lin, J. D. Protasiewicz, E. T. Smith and T. Ren, *Inorg. Chem.*, 1996, **35**, 6422–6428.
32 V. R. Preedy, *Betaine: chemistry, analysis, function and effects*, Royal Society of Chemistry, 2015.
33 R.-S. Tsai, B. Testa, N. El Tayar and P.-A. Carrupt, *J Chem Soc Perkin Trans 2*, 1991, 1797–1802.
34 W. E. Geiger and F. Barrière, *Acc. Chem. Res.*, 2010, **43**, 1030–1039.
35 Y.-Y. Wu, J.-D. Chen, L.-S. Liou and J.-C. Wang, *Inorganica Chim. Acta*, 2002, **336**, 71–79.

Experimental section, supporting data, and computational output coordinates have been uploaded as part of the supplementary information.